RUNX1 is a driver of renal cell carcinoma correlating with clinical outcome

Nicholas Rooney[1], Susan M. Mason[1], Laura McDonald[1], J Henry M. Däbritz[1], Kirsteen J. Campbell[1], Ann Hedley[1], Steven Howard[1], Dimitris Athineos[1], Colin Nixon[1], William Clark[1], Joshua D. Leach[1,2], Owen J. Sansom[1,2], Joanne Edwards[2], Ewan R. Cameron[3] and Karen Blyth[1,2*].

[1]CRUK Beatson Institute, Garscube Estate, Switchback Road, Bearsden, Glasgow, G61 1BD, United Kingdom, [2]Institute of Cancer Sciences, [3]School of Veterinary Medicine, University of Glasgow, Bearsden, Glasgow, G61 1QH.

Running title: RUNX1 and renal cell carcinoma

Key words: RUNX1, ccRCC, kidney cancer, RUNX2, GEM

Additional information:

*Corresponding author: Professor Karen Blyth, CRUK Beatson Institute, Garscube Estate, Switchback Road, Bearsden, Glasgow, G61 1BD UK. Telephone: +44 141 330 3686. Fax: +44 141 942 6521.
Email: Karen.Blyth@glasgow.ac.uk

The authors declare no potential conflicts of interest.

Word count: 4562 (+ 1881 Methods); Six main figures, two tables and five supplementary figures.

Abstract

The recurring association of specific genetic lesions with particular types of cancer is a fascinating, and largely unexplained area of cancer biology. This is particularly true of clear cell renal cell carcinoma (ccRCC) where although key mutations such as loss of VHL is an almost ubiquitous finding, there remains a conspicuous lack of targetable genetic drivers. In this study, we have identified a previously unknown pro-tumorigenic role for the RUNX genes in this disease setting. Analysis of patient tumor biopsies together with loss of function studies in preclinical models established the importance of RUNX1 and RUNX2 in ccRCC. Patients with high RUNX1 (and RUNX2) expression exhibited significantly poorer clinical survival compared to patients with low expression. This was functionally relevant as deletion of RUNX1 in ccRCC cell lines reduced tumor cell growth and viability in vitro and in vivo. Transcriptional profiling of RUNX1-CRISPR-deleted cells revealed a gene signature dominated by extracellular matrix remodelling, notably affecting STMN3, SERPINH1, and EPHRIN signaling. Finally, RUNX1 deletion in a genetic mouse model of kidney cancer improved overall survival and reduced tumor cell proliferation. In summary, these data attest to the validity of targeting a RUNX1-transcriptional program in ccRCC.

Significance: These data reveal a novel unexplored oncogenic role for RUNX genes in kidney cancer and indicate that targeting the effects of RUNX transcriptional activity could be relevant for clinical intervention in ccRCC.

Introduction

Kidney cancer is the 7th commonest cancer in the United Kingdom with around 12500 diagnoses and 4500 deaths annually (Cancer Research UK; www.cancerresearchuk.org; accessed July 2019). Around 85% of kidney cancers are classified as renal cell carcinomas (RCC) of which clear cell renal cell carcinoma (ccRCC) accounts for the vast majority (75%+) (1,2). Since the mid 1970's age standardised kidney cancer mortality rates have increased by 74% while the incidence rate has increased by 85% in relative terms in the last 25 years (Cancer Research UK). Various environmental risk factors such as smoking, hypertension and obesity contribute to kidney cancer development, but there is also a strong genetic contribution to the development of the disease (3). Many of these genetic alterations lead to changes in the transcriptional profile of the kidney cancer cells (4,5).

Currently RCC represents a pressing clinical challenge due to its increasing incidence. Early stage non-metastatic RCC can be treated by partial or radical nephrectomy, however early stage disease is often asymptomatic resulting in patients more commonly presenting with advanced disease which has a much poorer prognosis (6). Standard of care for high risk, advanced metastatic or recurrent RCC involves targeted tyrosine kinase inhibitors (TKI) primarily against the VEGF and mTOR pathways, which have modest improvement over previous cytokine therapies (7,8). Recently, combinatorial use of TKI with immune checkpoint inhibitors against programmed cell death complex (PD1 and PDL1) have shown promising results in stage III clinical trials (9). However the outlook for high risk patients remains poor and there is both a need for novel biomarkers of poor prognosis and identifying targetable genetic drivers.

Foremost among the genetic alterations that occur in kidney cancer is the loss of the short arm of chromosome 3 which contains the tumour suppressors *VHL* and *PBRM-1, BAP-1, SETD2* and occurs in up to 90% of cases of ccRCC (10,11). VHL protein functions as an E3 ubiquitin ligase targeting the hypoxia inducible factor (HIF) family of transcription factors for proteasomal degradation. Loss of VHL therefore causes a transcription factor driven change in gene expression leading to the

development of kidney cancer (1). The other tumour suppressor genes commonly deleted (*PBRM-1*, *BAP-1*, *SETD2*) all act directly or indirectly, through epigenetic changes in methylation status, to cause alterations in gene expression of kidney cancer cells (12). While much remains unknown about the transcription factors important for kidney cancer, these genetic alterations highlight the important role transcriptional misregulation plays in kidney cancer and the pressing need to identify the key factors involved.

RUNX1 is a member of an evolutionarily conserved family of *RUNX* genes that encode transcription factors. Together with its heterotypic binding partner CBFβ, RUNX1 forms a DNA binding complex required for normal mammalian development (13). RUNX1 also has established roles in various types of cancer (14) where classically, *RUNX1* chromosomal translocations and mutations are key drivers of haematopoietic malignancies and leukaemia (15). Increasingly however, RUNX1 has been shown to play 'context dependent' roles in solid tumours such as in the breast, where both *RUNX1* gain and loss of function has been associated with cancer (16-19). *RUNX1* has also been implicated in cancers of the ovary and uterus (20), prostate (21) and skin. To date, very little is known about a functional role for RUNX1 in either normal kidney development or kidney cancer. There is some evidence of increased expression of a *RUNX1* chromosomal translocation product in ccRCC patient samples (22) and RUNX1 has been shown to be expressed in mouse models of kidney fibrosis (a feature of chronic kidney disease correlated with RCC), involving RUNX regulation of TGFβ driven EMT (23).

Here we show that RUNX1 is expressed in human ccRCC and that high protein expression correlates with poorer survival. This is functionally relevant as deletion of *RUNX1* in human ccRCC cell lines disrupted tumour cell growth *in vitro* and *in vivo,* and enabled identification of a novel set of RUNX1 dependent genes in ccRCC. By utilising a genetically engineered mouse (GEM) model of kidney cancer we were able to interrogate the role of RUNX1 in tumour formation and genetically confirm that *in vivo* deletion of *Runx1* slows kidney cancer development. Finally, we reveal that the related

transcription factor RUNX2 is expressed in ccRCC, also associating with poorer survival. Our results provide the first evidence that RUNX proteins are novel players in kidney cancer and functionally contribute to disease progression and clinical outcome.

Materials and Methods

Antibodies

RUNX1 (8529), RUNX2 (8486), GAPDH (3683), HRP-conjugated anti Rabbit secondary antibody (7074) Cell Signaling Technology; SERPINH1 (10875-1-AP), Stathmin3 (11311-1-AP) ProteinTech. Primary antibodies used for immuno-blotting at 1:1000 dilution. Ki67 SP6 (RM-9106-S) Thermo Fisher Scientific.

Immunoblotting

Cells lysed in Pierce™ RIPA buffer (Thermo Scientific), protein extracts resolved on 10% NuPAGE Novex Bis-Tris gels (Life Technologies) and transferred to Hybond-ECL nitrocellulose membranes (Amersham). All membranes stripped and re-probed for GAPDH.

Immunohistochemistry and analysis

Immunohistochemical (IHC) staining for RUNX1/RUNX2 performed on 4µm formalin fixed paraffin embedded (FFPE) sections previously dry heated at 60^{o}C for 2 hours. IHC performed on Agilent Autostainer link48. Sections manually dewaxed through xylene, graded alcohol, tap water before heat-induced epitope retrieval (HIER) with sections heated to 98^{o}C (25 mins); rinsed in Tris buffered saline with Tween (TBST), peroxidase blocked (Agilent, UK), washed in TBST before application of antibody at previously optimised dilution (RUNX1 1:75, RUNX2 1:300) for 40 minutes. Sections washed in TBST before application of rabbit EnVision (Agilent, UK) secondary antibody for 35 minutes and rinsed in TBST before applying Liquid DAB (Agilent, UK) for 10 minutes. Sections washed in water, counterstained with haematoxylin and cover-slipped using DPX. Ki67 (1:200 dilution); SERPINH1 (1:80 dilution and high pH antigen retrieval). Digital images captured on a Leica SCN400f slide-scanner (x20). Quantification of Ki67 performed manually using HALO image analysis software (Indica Labs).

Tissue microarray

The tissue microarray (TMA) contained cores from 184 patients diagnosed with ccRCC within the Greater Glasgow NHS Trust between 1997 and 2008 and obtained from Greater Glasgow and Clyde NHS Biorepository as described previously (24,25). Briefly, to address tumour homogeneity, three cores measuring 0.6mm^2 from three different tumour-rich areas, as identified by a specialist pathologist, were used to construct the 3 TMAs. After IHC for RUNX1 or RUNX2 (above) and haematoxylin co-staining, the proportion of tumour cells with RUNX nuclear positivity was manually quantified using the weighted histoscore (H-Score) method. This involved calculating a semi-quantitative score by multiplying the percentage of cells showing staining by a score ranging from 0-3 representing increasing intensity of staining (Score 0-no staining, Score 1-weak staining, Score 2-moderate staining and Score 3-strong staining) providing a score from 0 to 300 (25). Three TMA sections were stained at the same time and average H-Scores obtained. H-Scores were stratified into quartiles (Q1-Q4), the upper quartile Q4 assigned as RUNX-High and remaining quartiles Q1-3 assigned as RUNX-Low. One third of the TMA was independently scored and agreement assessed by Interclass correlation coefficient >0.8 (26). Klintrup-Makinen score is a pathologically defined measure of inflammatory infiltration described previously for this TMA (24,25,27). Statistical analysis performed using SPSS Statistics Version 21.0 (SPSS IBM, NY). Associations between categorised H-scores and available data on variables were analysed using X^2-tests. Kaplan-Meier curves plotted with corresponding log-rank tests to assess the relationship between these markers and survival. Multivariate analysis was performed using backwards Cox regression conditional technique to test for independence (25).

Cell Lines

786-O cells (cultured in RPMI medium), Caki-2 cells (cultured in McCoy's 5a medium (Sigma)) and HEK293 cells (cultured in DMEM) were provided by Professor Eyal Gottlieb, (Beatson Institute, 2014). All media supplemented with 10% FCS, 2mM L-Glutamine, Penicillin/Streptomycin and 0.5µg/ml Amphotericin B (Sigma). All media reagents from Gibco unless otherwise stated. Cells were

of low passage and cultured for approximately 2 months after recovery from frozen vials. RCC cell lines (786-O & Caki-2) were authenticated using Promega GenePrint 10 system Short Tandem Repeats (STR) multiplex assay that amplifies 9 tetranucleotide repeat loci and the Amelogenin gender determining marker (December 2016). Cells routinely tested for mycoplasma.

shRNA and CRISPR/CAS9 RUNX1 gene silencing

RUNX1 MISSION© shRNA lentivirus DNA constructs (Sigma) used for targeting human *RUNX1* (sh1: TRCN0000338489, sh5: TRCN0000013660). Lentiviruses produced by transfecting HEK293 cells with 10µg of the relevant shRNA expression vector (pLKO) with 7.5µg PsPax2 and 4µg pVSVG packaging vectors (Tronolab) using the Calcium Chloride method; complete medium replacement 5 hours after transfection. 48 hours after transfection viral supernatant was removed, sterile filtered (0.45µm pores) and used to infect adherent 786-O and Caki-2 cells overnight in the presence of 8µg/ml Polybrene (Sigma). Live cell visualisation of GFP confirmed successful transduction. Cells were maintained in medium containing 2µg/ml Puromycin (Sigma). For CRISPR/CAS9 deletion, guide RNAs (gRNA) targeting human *RUNX1* were designed using the Zhang Lab tool (MIT, USA). The gRNA sequence used was 5'-ATGAGCGAGGCGTTGCCGCT-3'. 786-O cells were transfected using lipofectamine (Thermo Fisher); 8µl of Lipofectamine in 250µl serum free medium (SFM) and 2µg DNA in 250µl of SFM (with GLN), were each left for 10 minutes at room temperature then the Lipofectamine/DNA mix incubated at RT for 30 min before being added to $2x10^5$ 786-O cells (plated overnight) and incubated at 37°C for 5 hours prior to a medium change. 48 hours after transfection cells were cultured in medium containing 2µg/ml Puromycin for 48 hours. Transfected cells grew back as individual colonies, which were picked, expanded and screened for RUNX1 deletion by immunoblotting.

Cell growth assays (cell counting, xCELLigence and MTS)

$2x10^4$ 786-O (pX Ctrl) and 786-O RUNX1 CRISPR clones (CRISPR A1/CRISPR A3) were plated in triplicate in 12-well plates, trypsinised and counted using the Casyton cell counter 96 hours later.

Cell count for pX Ctrl cells were normalised to 1 and CRISPR clones expressed as a proportion, experiments were repeated at least 4 times. $7x10^3$ Caki-2 cells were plated and counted as above. For xCELLigence assay $3x10^3$ 786-O cells were plated in quadruplicate into wells of an E Plate 16. The impedance applied to an electric field over time caused by cells growing in the plate is proportional to the number of cells in the plate which is represented as a cell index when measured using the XCELLigence Real Time Cell Analysis System (Roche Diagnostics GmbH, Mannheim, Germany). Experiments performed in quadruplicate at least 3 times with separate batches of cells. For MTS cell viability assays $3x10^3$ 786-O cells or $1x10^3$ Caki-2 cells were plated in quadruplicate in 96 well plates, every 24 hours a 20% volume of CellTiter96 MTS assay reagent (Promega) was added per well and incubated for 1 hour prior to reading absorbance at A490. Experiments repeated at least three times with separate batches of cells.

EdU pulse chase

$1x10^5$ 786-O cells were left to adhere overnight in complete medium. Medium was removed and replaced with complete medium containing 10μM EdU and incubated at 37^OC for 30 minutes. Cells were washed twice in PBS and sampled immediately or 6 hours later. Cells were co-stained with 50μg/ml propidium iodide (Sigma) for 30 minutes with gentle rocking then analysed on an Attune NTX flow cytometer. All experimental conditions performed in triplicate three separate times. Flow cytometry data analysed using FlowJo.

Sytox© Green apoptosis assay

$3x10^3$ 786-O cells were plated (24 well plate) and allowed to adhere overnight. The next day medium was changed to complete medium containing 5μM of Sytox© Green. The plate was imaged every hour for 68 hours on an Incucyte FLR imaging system. Confluence and number of Sytox© positive cells per well were calculated using Incucyte software.

Scratch wound assay

786-O cells were plated in a 96 well image lock plate and allowed to adhere overnight in complete medium. At confluence the plate was scratched using the wound-maker (Essen Biosciences) and medium changed. Closure of the wound was imaged every hour over 24 hours and analysed using Incucyte ZOOM live cell imaging system. All experiments performed in quadruplicate 3 times.

Animal studies

All animal experiments performed under UK Home Office Project Licences (60/4181 & 70/8645) with ethical approval from the Beatson Institute and the University of Glasgow under the Animal (Scientific Procedures) Act 1986 and EU directive 2010. Mice were maintained in purpose built facility in a 12-hour light/dark cycle with continual access to food and water.

Kidney capsule xenograft

8-10 week old female CD1-Foxn1^{nu} (nude) mice obtained from Charles River (UK). 5x10^{5} 786-O* cells were injected directly into the kidney capsule in 20µl growth factor reduced Matrigel. Mice were continually assessed for signs of kidney impairment, and kidney tumour development monitored by Ultrasound Imaging. Mice were humanely sacrificed at clinical endpoint or 18 week time-point. Parental 786-O cells were initially passaged once *in vivo* through the kidney (as described above) and a secondary 786-O cell line (referred to as 786-O*) was established in culture using an adapted version of the method described here (28). Briefly, the kidney was excised and normal tissue removed. The tumour was finely chopped into a paste and incubated with 140rpm rotation at 37^{O}C for ten minutes in 10ml of 1mg/ml Type 2 collagenase (Sigma). The tube was vortexed vigorously for 30 seconds before a second ten minute incubation. Cells were washed with RPMI and passed through sequential 100, 70 and 40µm filters. *RUNX1* was deleted from the 786-O* line by CRISPR/CAS9 as described above. 786-O* vector control and CRISPR cells were confirmed to not express CAS9 prior to engraftment.

RNA sequencing

239 5x10^5 786-O cells (pX Ctrl, CRISPR A1 and CRISPR A3) were plated and sampled 48 hours later. Whole
240 RNA extracted using RNeasy mini kit (Qiagen) according to manufacturer's protocol. RNA was DNAse
241 treated using RNAse free DNAse set (Qiagen). RNA quality was tested on an Agilent 2200 Tapestation
242 using RNA screentape, all RNA integrity value ≥9.6. Libraries for cluster generation and DNA
243 sequencing were prepared following an adapted method from Fisher et al (29) using Illumina TruSeq
244 Stranded mRNA LT Kit. Quality and quantity of DNA libraries assessed on an Agilent 2200
245 Tapestation (D1000 screentape) and Qubit (Thermo Fisher Scientific) respectively. Libraries were run
246 on Illumina Next Seq 500 using High Output 75 cycles kit (2x36cycles, paired end reads, single index).
247 Quality checks on raw RNA-seq data files done using fastqc version 0.11.7 and fastq_screen version
248 0.11.4. RNA-seq paired-end reads were aligned to the GRCh38 (30) version of the mouse genome
249 using tophat2 version 2.1.0 with Bowtie version 2.2.6.0. Expression levels determined and
250 statistically analysed by a combination of HTSeq version 0.6.1, the R environment, version 3.5.0,
251 utilizing packages from Bioconductor data analysis suite and differential gene expression analysis
252 based on the negative binomial distribution using DESeq2. Full data sets produced from this study
253 are publically available on the Sequence Read Archive database, accession number: PRJNA605312.

254 **GEM model of kidney cancer**

255 *Cyp1aCre; Apc$^{fl/fl}$; p21$^{-/-}$* mice (hereafter referred to as *CAP*) were characterised in the Sansom lab as
256 described previously (31). These mice were crossed with *Runx1$^{fl/fl}$* mice (32) (a kind gift from Dr
257 Nancy Speck, Jax:010673, B6;129-*Runx1$^{tm3.1Spe/}$*J) and/or *Runx2$^{fl/fl}$* mice (33). Tumour mice (equivalent
258 numbers males/females in each cohort) were monitored for signs of tumour development and
259 subsequently checked 3 times a week for signs of endpoint renal failure (blood in urine, hunching,
260 swollen kidneys)(31). At endpoint kidneys were fixed in 10% neutral buffered formalin and
261 embedded in paraffin for subsequent histological analyses.

262 **Statistical Analyses**

263 The TMA was analysed using SPSS. All other statistical analyses were performed using
264 Graphpad/PRISM. The specific statistical tests used are indicated throughout. All error bars
265 represent -/+ SEM unless otherwise indicated.
266
267
268
269
270
271
272
273
274
275
276
277
278
279
280
281
282

Results

RUNX1 is expressed in human ccRCC and correlates with poor survival and increased inflammation

In silico analysis of The Cancer Genome Atlas (TCGA) ccRCC dataset (5) revealed that *RUNX1* alterations occur in 6% of ccRCC cases and strikingly, the vast majority of these alterations are mRNA upregulations (96%) (Supplementary Fig1a). A 6% alteration rate is comparable with the rate at which other established genes involved in ccRCC are altered (34) such as *MTOR* (11%), *PI3KCA* (8%), *PTEN* (8%), *TP53* (7%), while interestingly, the pattern of alterations is much more varied for these genes (Supplementary Fig1b). Kaplan-Meier survival analysis of the ccRCC patients with *RUNX1* mRNA upregulation shows that they have a statistically significant decrease in survival compared to the unaltered cohort (Log-rank P=0.0008, *RUNX1* Unaltered median=76.98 months, *RUNX1* mRNA upregulation median=36.21 months) (Supplementary Fig1c). This is in line with a recent report interrogating the TCGA dataset (35). Furthermore, data obtained using the pan-cancer RNA-seq KM plotter (36) tool analysing clinical survival data from 530 ccRCC patients also show that high *RUNX1* expression correlates with poorer overall survival (P<0.0001), (Supplementary Fig1d).

Tissue microarrays (TMA) have previously been used to investigate the protein expression level of RUNX1 in human epithelial tumours of the breast (17,37) and ovary (38). Therefore, as an independent validation of *in silico* observations we immuno-stained a TMA containing 184 tumour samples from ccRCC patients. RUNX1 is clearly expressed in cell nuclei in a subset of ccRCC patient samples and is not expressed in the non-tumour kidney sample contained within the TMA (Fig1a). RUNX1 staining was scored by the weighted average histoscore (H-Score) method to quantify the range of RUNX1 expression (see methods). The TMA was stratified into quartiles and the upper quartile (RUNX1-High, H-Score: 30 to 225, mean=87.5, n=46) was compared to the remaining lowest scoring cores (RUNX1-Low, Q1-Q3 H-Score: 0-26.7, mean=4.1, n=138) (Fig1b). Patient survival information was available for 183 patients, Kaplan-Meier survival analysis revealed that RUNX1-high patients had a significantly poorer cumulative survival than RUNX1-low patients, Log-rank P=0.007

(Fig1c). The survival rate was consistently lower year on year and at 5 years from diagnosis was 68% for RUNX1-high patients compared to 88% for RUNX1-low, Wilcoxon p=0.005 (Fig1c). Assessment of clinico-pathological characteristics showed that there was no significant association with RUNX1 H-Score and age, grade, necrosis or recurrence (Table1). However high RUNX1 expression was significantly associated with a high Klintrup-Makinen (KM) score, a pathologically defined measure of inflammation previously described for this TMA (see methods). The average RUNX1 H-Score was significantly higher for patients with a high KM score compared to low (34.1 vs 15.2, T-test P= 0.0027) (Fig1d). Accordingly, RUNX1-high patients were distributed 28% KM low vs 72% KM high, compared to 55% KM low vs 45% KM high for RUNX1-low patients (Fig1e). These data reveal for the first time that RUNX1 protein is aberrantly expressed in human ccRCC and that high RUNX1 expression is an independent marker of poor prognosis (P=0.027, hazard ratio 1.58: 95% 1.054-2.372) when combined with age, stage, grade and tumour necrosis. These data also reveal that RUNX1-high patients have an increase in inflammatory infiltration compared to their RUNX1-low counterparts.

RUNX1 is expressed in human ccRCC cell lines and deletion reduces cell growth

Having conclusively shown that RUNX1 expression correlates with poorer survival in ccRCC we wanted to ascertain a functional role for RUNX1 in this disease setting. To this end RUNX1 expression was modulated in human ccRCC cell lines. Lentiviral delivery of different short hairpin RNAs (shRNA) was used to knockdown RUNX1 expression in 786-O and Caki-2 cells (sh1 and sh5) compared to a scrambled control shRNA (Scr) (inset Fig2a and Supplementary Fig2a). shRNA mediated knockdown of RUNX1 caused a decrease in cell index (proportional to the number of adherent viable cells) over a 125h period in culture in the 786-O cell line as assayed using the xCELLigence assay system (Fig2a-b). Cell number was also significantly reduced in a second cell line (Caki-2) with RUNX1 knockdown (Fig 2c). In addition, cell viability after RUNX1 knockdown in 786-O and Caki-2 cells was reduced as assessed by the MTS assay (Supplementary Fig2b-c). To validate

these findings 786-O cells were transfected with gRNA targeting *RUNX1*, and CAS9 nuclease. Complete knockout of RUNX1 protein was confirmed in 786-O RUNX1 CRISPR clones (CRISPR A1 and CRISPR A3) by immunoblot (inset Fig2d). CRISPR deletion of RUNX1 also caused a more pronounced decrease in cell index (Fig2d-e) and a decrease in cell number (Fig2f) in both 786-O CRISPR clones.

To understand the nature of the growth defect observed in the RUNX1 knockout cells, the rate at which they were actively synthesising DNA by incorporation of the thymidine analogue EdU was assessed. 786-O control and RUNX1-deleted cells were pulsed with EdU by incubation for 30 minutes in medium containing EdU, then sampled by fixation in 4% PFA immediately after EdU incubation (T0) or 6 hours later (T6). The cells were co-stained for EdU and PI (Propidium Iodide) and analysed by flow cytometry as shown for the T6 time-point (Fig2g). There was no difference in total EdU incorporation between control and RUNX1-deleted cells at T0 (Supplementary Fig2d) and at T6 (Fig2h). However there was a clear reduction in the G1* population representing EdU+ve cells which have transitioned through S-phase and returned to G1 in both the RUNX1–deleted cell lines (Fig2i and population highlighted in box in Fig2g). This suggests that the RUNX1-deleted cells face a delay in transitioning through the S/G2 stages of the cell cycle. Finally, the number of dead cells was assessed by time-lapse imaging of the control and RUNX1-deleted cells in the presence of SYTOX® Green nucleic acid stain. This revealed that the number of SYTOX® positive dead cells per well, as a proportion of % confluence, was higher in the RUNX1-deleted cells compared to control, especially at earlier time-points (Fig2j). Confluence and the number of SYTOX® positive dead cells per well are shown individually in Supplementary Fig2e-f. Together, these data indicate that knockout of RUNX1 causes a reduction in cell growth in ccRCC cell lines and that RUNX1 CRISPR cells have a subtle delay in progression through the cell cycle and an increase in cell death.

Knockout of RUNX1 in 786-O ccRCC cells reduces* in vitro *cell migration and* in vivo *tumour formation

To further investigate the effect of RUNX1 knockout in physiologically relevant assay systems, the effect of deletion on cell migration using *in vitro* scratch-wound assays was assessed. This revealed that RUNX1 deleted cells exhibited decreased wound closure and reduced relative wound density over a 24h period (Fig3a-c). To establish whether RUNX1 deletion effects ccRCC development *in vivo*, and to circumvent the low tumourigenicity of the 786-O cell line, we generated a secondary cell line (hereafter referred to as 786-O*) by passaging 786-O cells through the kidney *in vivo* (see methods). RUNX1 was deleted in these 786-O* cells by CRISPR/CAS9 as performed above (Supplementary Fig3a) and these 786-O* RUNX1-deleted cells showed a similar growth defect to the parental cells (Supplementary Fig3b-c). RUNX1-deleted and control 786-O* cells were injected directly into the kidney capsule of CD1-*Nu/Nu* recipient mice and their tumour growth was monitored by ultrasound over an 18 week period. This revealed that at 10 weeks post-surgery 7/13 mice injected with the control cells had formed tumours compared to 0/13 for the RUNX1-deleted 786-O* cells (Fig3d). When sacrificed at 18 weeks, 8/13 mice injected with RUNX1-proficient cells had grossly observable kidney tumours whereas just 1/13 of the recipients with RUNX1-deleted cells had a small tumour growth (p=0.011; Fishers Exact Test; Fig3d & Supplementary Fig3d). Four out of thirteen control mice exhibited gross lung metastases whilst none of the RUNX1-deleted group did. Kidney tumours from the control group and the single tumour arising in the RUNX-1 deleted cohort were stained for RUNX1 and its closely related family member RUNX2. RUNX1 was highly expressed in all control tumours tested (n=4) while it was absent from the RUNX1-deleted tumour as expected (Fig3e). However it was notable that RUNX2 was present in both control and RUNX1-deleted tumours. These data support our findings that RUNX1 is important for growth and survival of human ccRCC cells and that deletion of RUNX1 hampers tumour growth and development *in vivo*.

Identification of a RUNX1 regulated gene signature in ccRCC

As RUNX1 deletion causes a defect in ccRCC cell growth we wanted to understand the significant downstream players by assessing how deletion of RUNX1 effects the global transcriptional profile in

human 786-O ccRCC cells. RNA sequencing was performed on whole RNA extracts from control and RUNX1 CRISPR cells (as used in Figure 2). Several hundred genes were significantly differentially expressed (P<0.05, >2fold up or down regulation) in either RUNX1-deleted cell line (A1=1185, A3=1296). This revealed a novel RUNX1 regulated signature of 724 genes common to both clones that were significantly differentially expressed, with 710 altered in the same direction in both RUNX1 CRISPR clones compared to the control cells (Fig4a). Excluding uncharacterised genes, pseudogenes and novel transcripts, 661 genes are significantly differentially expressed with 394 upregulated and 267 downregulated on RUNX1 deletion in both clones. Principle component analysis revealed exceptionally high agreement between the datasets with 97% of the variance explained by RUNX1 deletion (Supplementary Fig4). Full lists of the regulated genes are available in supplementary data file 1 where they are ranked by fold-change and significance. Gene ontological analysis using Metacore revealed the main biological pathways that were altered on RUNX1 deletion. This encompasses a range of pathways such as cell adhesion and ECM remodelling, Eph and Ephrin signalling, angiogenesis and Glutathione metabolism (Fig4a). The most altered pathway was *cell adhesion and ECM remodelling* which included changes in expression of genes such as *MMP1, MMP16, SERPINE2, Fibronectin and Syndecan 2* (Fig4b). The average fold change on the x axis (x=Average log2(Fold Change)) was plotted against significance on the y axis (y=-log10(Max(adjusted P values)) in a volcano plot to visually depict the most significantly differentially expressed genes (Fig4c). Two such genes, *STMN3*, which encodes a protein that plays a role in microtubule dynamics in the cell cycle (upregulated +46.3x, red circle Fig4c) and *SERPINH1* (HSP-47), increased expression of which has been shown to be a marker of poor prognosis in ccRCC (downregulated -4.1x, blue circle Fig4c) were validated by western blot which supported the findings of the RNA-seq data (Fig4d). Interestingly, the second most altered gene ontology was *Eph and Ephrin signalling* which are downstream targets of the WNT signalling pathway which is itself modulated by RUNX1 activity (Fig4e). Finally *CPT1A* which has been shown to be supressed in ccRCC was increased on RUNX1 deletion (Fig4f). These data have, for the first time, identified a group of genes whose expression is

significantly altered as a consequence of the level of RUNX1 in human ccRCC. This shows that deregulation of RUNX1 expression affects a wide range of key pathways, many of which are related to kidney cancer and cancer progression.

RUNX1 deletion improves survival in a genetic mouse model of kidney cancer.

To further explore the functional role of RUNX1 in a physiological setting we turned to a genetically engineered mouse (GEM) model where we could intrinsically modulate RUNX1 levels. First we ascertained the levels of RUNX1 in a GEM model of kidney cancer available in our lab in which Cre recombinase expressed in the kidney epithelium drives deletion of the tumour suppressor *Apc* on a p21 null background (31). Normal kidneys and kidney tumours from this model (*AH-Cre;Apc*$^{fl/fl}$*;p21*$^{-/-}$ referred to as *CAP*) were stained for RUNX1 to reveal that while RUNX1 is not expressed in normal kidney, it is significantly upregulated in kidney tumours (Fig5a). We proceeded to cross this *CAP* model with a conditional knockout of *Runx1* (*Runx1*$^{fl/fl}$) (32). RUNX1 deletion in the tumours of *CAP;Runx1*$^{fl/fl}$ mice was confirmed at the protein level by immunohistochemistry (IHC) which showed absence of RUNX1 (Fig5b). Cohorts of *CAP;Runx1*$^{+/+}$ and *CAP;Runx1*$^{fl/fl}$ mice were aged until clinical endpoint. Kaplan-Meier analysis shows that survival of *CAP;Runx1*$^{fl/fl}$ mice was significantly extended (Log-rank P= 0.0365) compared to their *CAP;Runx1*$^{+/+}$ counterparts, with a mean survival of 104.6 vs 78.6 days, t-test P= 0.0415 (Fig5c-d). Tumours were immuno-stained for the proliferation marker Ki67, which exhibited lower positive staining in tumours from the *CAP;Runx1*$^{fl/fl}$ mice compared to *CAP;Runx1*$^{+/+}$ (Fig5e). This was confirmed by quantification using the HALO imaging platform, which revealed that tumours from *CAP;Runx1*$^{+/+}$ mice had a higher proportion of Ki67+ve cells than from *CAP;Runx1*$^{fl/fl}$ mice (34% vs 24.4%, t-test P= 0.0154) (Fig5f). Finally, tumours immuno-stained for SERPINH1 (down-regulated in RNA-seq, Fig4e) revealed SERPINH1 is highly expressed in *CAP;Runx1*$^{+/+}$ tumours compared to normal kidney (Fig5g). Deletion of RUNX1 causes a significant decrease in SERPINH1 levels in kidney tumours in line with our RNA-seq data. Taken together, these

data from our GEM model of kidney cancer confirm *in vivo* that deletion of RUNX1 leads to improved survival and less tumour proliferation.

High RUNX2 expression also correlates with poorer survival in human ccRCC

Whilst deletion of *Runx1* significantly delayed tumourigenesis in the GEM model these animals still succumbed to disease. We hypothesized that the related RUNX family protein RUNX2 might be expressed and contribute to disease progression. Indeed RUNX2 was expressed both in the *CAP*;*Runx1*$^{+/+}$ and *CAP*;*Runx1*$^{fl/fl}$ tumours (Fig6a). Attempts to model deletion of RUNX2 in this model of kidney cancer were hampered by the non-viability of *AH-Cre;Runx2*$^{fl/fl}$ mice (suggesting a possible limiting requirement for RUNX2 in embryonic development). Heterozygous deletion of *Runx2* did not affect survival either on a *Runx1*$^{+/+}$ or *Runx1*$^{fl/fl}$ background in the *CAP* model. Although, it is important to note that RUNX2 protein expression was still observed in these tumours (Supplementary Fig5a-d). Interestingly however, *in silico* analysis of RUNX2 expression in the TCGA human ccRCC data set (5) revealed that *RUNX*2 is altered in 8% of ccRCC patients (93.5% are mRNA upregulations, Supplementary Fig5e). The pan-cancer RNA-seq KM plotter tool (described in Supplementary Fig1c) revealed human ccRCC patients with high RUNX2 expression had poorer survival (Log-rank P= <0.0001), (Supplementary Fig5f). It is noteworthy that *RUNX3* is also upregulated in ccRCC however, unlike *RUNX1* and *RUNX2,* it does not significantly correlate with disease-free survival (Supplementary Fig 5e-f). To directly assess the expression of RUNX2 in human ccRCC patients, the same TMA in Fig1 was used to show that RUNX2 protein is also expressed in human ccRCC (Fig6b). While the RUNX2 H-Score was on average lower than RUNX1 (Supplementary Fig5g), when stratified into quartiles based on RUNX2 H-Score (Supplementary Fig5h) patients with high RUNX2 also had a statistically significant decrease in survival compared to patients with low or no RUNX2 expression, Log-rank P= 0.0478 (Fig6c). At five years post diagnosis, survival for the RUNX2 Low quartile was 87% compared to 73% for RUNX2 High (inset table Fig6c). A positive correlation between RUNX1-High and RUNX2-High expression was also observed (Supplementary

Fig5i). Assessment of clinico-pathological characteristics for RUNX2 expression also showed no correlation with age, grade, necrosis and recurrence (Supplementary table 1). However similar to RUNX1, RUNX2 also correlated with a high KM score (Fig6d-e). These data reveal that the related transcription factor RUNX2 is also important in human ccRCC with high expression being indicative of a poorer prognosis.

Taken together, we have identified a novel role for the RUNX family of transcription factors in kidney cancer where both RUNX1 and RUNX2 are expressed and act in an oncogenic fashion that aids the progression of the disease.

Discussion

This study underscores the importance and functional relevance of the developmentally important transcription factor RUNX1 in kidney cancer. Interrogation of The Cancer Genome Atlas shows *RUNX1* to be upregulated in ccRCC (this study and (35,39)) which we can now corroborate using histochemical analysis of an independent cohort. ccRCC patients with poor prognosis have high RUNX1 expression, while deletion of RUNX1 reduced kidney cancer cell growth and prevented or delayed tumour development. In addition we have shown for the first time that RUNX2 is also expressed in patients with poor prognosis. This work opens up a new and unexplored avenue of research into the *RUNX* genes' enigmatic functions in neoplastic disease and identifies the *RUNX* genes as novel players in the genetic landscape of kidney cancer.

Initial gene expression observations *in silico* revealed that alterations in *RUNX1* occur at a similar frequency as perturbation of other kidney cancer drivers. Strikingly, almost all *RUNX1* alterations were mRNA upregulations, suggesting increased expression is the mode by which RUNX1 contributes to ccRCC. RUNX1 activity appears to be associated with the neoplastic state in renal cells as normal tissues show little evidence of expression. This may reflect the specific ccRCC transcriptome, defined by the recurring molecular changes that typify this disease. Given the importance of Hypoxia Induced Factor (HIF) activation in the pathogenesis of this disease it is worth noting that a number of studies have pointed to the interplay between HIFs and RUNX transcription factors including: physical interaction; co-regulation of target genes; and in the case of RUNX2, stabilisation of the HIF protein (40-42). Moreover, the *RUNX* genes are themselves regulated by HIFs, raising the possibility that they are both downstream targets, and act to potentiate the oncogenic signal (43). Molecular characterisation of RCC subtypes revealed that increased immune cell infiltration gene expression signatures associated with the poorest performing patients specifically in ccRCC (4,44,45) and immune checkpoint inhibitors are currently in clinical trial for advanced disease (8,9). In this regard it is interesting that our study reveals a positive correlation between RUNX and

local inflammatory cell infiltration. Increased systemic inflammation is a known feature of renal cancer (46,47) and integration of Klintrup-Makinen score with systemic biomarkers was able to predict poor prognosis in ccRCC (27). Gene ontology profiles suggest that immune and inflammatory processes dominate the expression landscape of ccRCC (10,11).

RUNX1 deletion in ccRCC cell lines perturbed the cell cycle and reduced cell viability while *Runx1* deletion in our GEM model decreased tumour growth and tumour cell proliferation. This genetically confirmed an oncogenic role for RUNX1 which was also highly upregulated in another murine model of ccRCC (48). There is considerable evidence that RUNX1 has an important role in proliferation in organisms as diverse as nematodes (49), sea urchins (50) and mammals; although whether it promotes or restricts cell division depends on the cellular context (51,52). Similarly RUNX1 is known to regulate cell survival differently in different cell types (53,54), and downstream mediators of survival have been identified in some tissue systems (55). Our cell line data is given greater physiological relevance by the observation that *RUNX1* null ccRCC cells almost entirely failed to grow in a kidney xenograft model. Further, our data showing a pro-proliferative effect in cell lines and tumours together with enhanced cell survival suggests an exclusively oncogenic role for RUNX1 in the context of renal cancer cells.

Using RNA sequencing we revealed that deletion of *RUNX1* induces profound gene expression changes. KEGG analysis of RCC expression profile studies have emphasised that upregulated genes are associated with significant cell adhesion changes and interactions between cytokines and their receptors (56). In this regard it is worth noting that our gene analysis showed enriched expression of genes involved in cell-ECM interactions and cell-cell interactions such as Eph-Ephrin signalling, suggesting RUNX1 may be contributing to a common oncogenic pathway in renal cancer. One of the most significantly down-regulated genes in our human *RUNX1*-deleted RCC cells and murine tumours was *SERPINH1*. Importantly, SERPINH1 is a potential negative prognostic marker in ccRCC (57) and is required for collagen folding and secretion (58), therefore its expression may contribute

to changes in tissue architecture that promote tumour development. SERPINH1 also associates with enhanced TGFβ signalling and both RUNX1 and RUNX2 have been shown to be involved in TGFβ induced kidney fibrosis (23,59). The role of collagen in ccRCC is currently unclear, however collagen density and alignment have recently been shown to be significantly higher in patients with high grade tumours compared to low grade (60). The fatty acid metabolism enzyme CPT1A increased markedly on *RUNX1* deletion suggesting a negative correlation. CPT1A is reduced in ccRCC where suppression causes lipid droplet accumulation (a prominent feature of ccRCC) and tumour development (61). Intriguingly, suppression of CPT1A in ccRCC is mediated by the HIF family and is therefore an example of potential RUNX1 interplay with the VHL-HIF signalling axis. We also observed a pronounced increase in STATHMIN3, a microtubule binding protein important for the formation of mitotic spindles. Over expression of STATHMIN3 has been associated with delayed cell cycle in leukaemia (62). Future studies using ChIP-seq analysis would provide valuable insights into which genes are directly modulated by RUNX activity and functionally contribute to the RUNX1-related phenotype in renal cells.

The long term trend for kidney cancer is one of growing global incidence, and improved treatments for advanced disease remains an unmet clinical need. Human patients with the highest RUNX1 expression in our study had the poorest prognosis and a 20% reduction in survival rate at 5 years post diagnosis (68% vs 88%). Indeed, RUNX1 associated with poorer survival independent of age, grade and stage. These data identify RUNX1 as a novel prognostic biomarker and as a potential therapeutic target in human ccRCC. This is encouraging given the active pursuit of therapeutic agents that can block the transcriptional function of the RUNX proteins (63). However the wider consequences of directly targeting RUNX in kidney cancer would need to be established in the context of the sustained requirement for RUNX function in other tissues.

In general, the relationship between the *RUNX* genes and other haematopoietic and solid tumours is complex with both a tumour suppressor and a pro-oncogenic role described in leukaemia (14,15),

546 breast (18) and prostate cancer (21). As such ccRCC may be the optimal choice for exploring novel
547 therapeutic agents that block RUNX function. This is further given credence considering that the
548 related family member RUNX2 is also associated with poorer survival and increased inflammation in
549 ccRCC patients, and was also highly expressed in our GEM model. Indeed RUNX1 and RUNX2 co-
550 occurred in a selection of patient samples as well as in GEM tumours. Although our staining was
551 carried out on serial sections, dual immunohistochemistry for both RUNX1 and RUNX2 could give
552 valuable insights into the spatial localisation and consequence of co-occurrence of the RUNX
553 transcription factors. Although beyond the scope of this study, it will be important to dissect this
554 interplay between the RUNX proteins in ccRCC and how they each contribute to the disease
555 phenotype. Furthermore, while we have not specifically investigated RUNX3 in our system, *in silico*
556 analysis revealed it is also upregulated in kidney tumours at the mRNA level. Intriguingly, akin to
557 that observed in pancreatic adenocarcinoma (64), transcriptomic upregulation of *RUNX3* did not
558 relate to patient survival. Nonetheless Whittle *et al* elegantly demonstrated that high RUNX3 in their
559 pancreatic cancer TMA did correlate with poor prognosis and conveyed a pro-metastatic phenotype.
560 Therefore it will be interesting to study RUNX3 further in the context of ccRCC to ascertain if its role
561 recapitulates that seen in pancreatic cancer. Future studies will use compound genetic models and
562 anti-RUNX drugs to investigate the consequence of total ablation of RUNX function in kidney cancer.

563

564

565

566

567

568

569

Acknowledgments

We would like to acknowledge the Core Services and Advanced Technologies at the Cancer Research UK Beatson Institute (C596/A17196), with particular thanks to the Biological Services Unit, Histology and Molecular Technologies. We thank the NHS Greater Glasgow and Clyde Biorepository for supplying the TMA; Tom Hamilton and Sandeep Dhayade for assistance with xenograft surgery; Professor Eyal Gottlieb for providing 786-O and Caki-2 cell lines and David Stevenson for advice on CRISPR strategy. We thank Catherine Winchester for critical reading of the manuscript. This work was funded by CRUK core funding C596/A17196 (KB and OJS labs - CRUK Beatson Institute) and Renal Cancer Research Fund Scotland (to JE) who supported the TMA production.

References

1. Nabi S, Kessler ER, Bernard B, Flaig TW, Lam ET. Renal cell carcinoma: a review of biology and pathophysiology. F1000Research **2018**;7:307-
2. Hsieh JJ, Purdue MP, Signoretti S, Swanton C, Albiges L, Schmidinger M*, et al.* Renal cell carcinoma. Nat Rev Dis Primers **2017**;3:17009
3. Tahbaz R, Schmid M, Merseburger AS. Prevention of kidney cancer incidence and recurrence: lifestyle, medication and nutrition. Curr Opin Urol **2018**;28:62-79
4. Ricketts CJ, De Cubas AA, Fan H, Smith CC, Lang M, Reznik E*, et al.* The Cancer Genome Atlas Comprehensive Molecular Characterization of Renal Cell Carcinoma. Cell Rep **2018**;23:313-26.e5
5. Comprehensive molecular characterization of clear cell renal cell carcinoma. Nature **2013**;499:43-9
6. Escudier B, Porta C, Schmidinger M, Rioux-Leclercq N, Bex A, Khoo V*, et al.* Renal cell carcinoma: ESMO Clinical Practice Guidelines for diagnosis, treatment and follow-updagger. Ann Oncol **2019**;30:706-20
7. Motzer RJ, Hutson TE, Tomczak P, Michaelson MD, Bukowski RM, Rixe O*, et al.* Sunitinib versus interferon alfa in metastatic renal-cell carcinoma. N Engl J Med **2007**;356:115-24
8. Ghali F, Patel SH, Derweesh IH. Current Status of Immunotherapy for Localized and Locally Advanced Renal Cell Carcinoma. J Oncol **2019**;2019:7309205
9. Motzer RJ, Penkov K, Haanen J, Rini B, Albiges L, Campbell MT*, et al.* Avelumab plus Axitinib versus Sunitinib for Advanced Renal-Cell Carcinoma. N Engl J Med **2019**;380:1103-15
10. Mitchell TJ, Turajlic S, Rowan A, Nicol D, Farmery JHR, O'Brien T*, et al.* Timing the Landmark Events in the Evolution of Clear Cell Renal Cell Cancer: TRACERx Renal. Cell **2018**;173:611-23.e17
11. Turajlic S, Xu H, Litchfield K, Rowan A, Horswell S, Chambers T*, et al.* Deterministic Evolutionary Trajectories Influence Primary Tumor Growth: TRACERx Renal. Cell **2018**;173:595-610.e11
12. Varela I, Tarpey P, Raine K, Huang D, Ong CK, Stephens P*, et al.* Exome sequencing identifies frequent mutation of the SWI/SNF complex gene PBRM1 in renal carcinoma. Nature **2011**;469:539-42
13. Okuda T, van Deursen J, Hiebert SW, Grosveld G, Downing JR. AML1, the target of multiple chromosomal translocations in human leukemia, is essential for normal fetal liver hematopoiesis. Cell **1996**;84:321-30
14. Ito Y, Bae SC, Chuang LS. The RUNX family: developmental regulators in cancer. Nat Rev Cancer **2015**;15:81-95
15. Sood R, Kamikubo Y, Liu P. Role of RUNX1 in hematological malignancies. Blood **2017**;129:2070-82
16. Ellis MJ, Ding L, Shen D, Luo J, Suman VJ, Wallis JW*, et al.* Whole-genome analysis informs breast cancer response to aromatase inhibition. Nature **2012**;486:353-60
17. Ferrari N, Mohammed ZM, Nixon C, Mason SM, Mallon E, McMillan DC*, et al.* Expression of RUNX1 correlates with poor patient prognosis in triple negative breast cancer. PLoS One **2014**;9:e100759
18. Rooney N, Riggio AI, Mendoza-Villanueva D, Shore P, Cameron ER, Blyth K. Runx Genes in Breast Cancer and the Mammary Lineage. RUNX Proteins in Development and Cancer. Singapore: Springer Singapore; 2017. p 353-68.
19. Banerji S, Cibulskis K, Rangel-Escareno C, Brown KK, Carter SL, Frederick AM*, et al.* Sequence analysis of mutations and translocations across breast cancer subtypes. Nature **2012**;486:405-9

20. Riggio AI, Blyth K. The enigmatic role of RUNX1 in female-related cancers - current knowledge & future perspectives. Febs j **2017**;284:2345-62
21. Takayama K, Suzuki T, Tsutsumi S, Fujimura T, Urano T, Takahashi S*, et al.* RUNX1, an androgen- and EZH2-regulated gene, has differential roles in AR-dependent and -independent prostate cancer. Oncotarget **2015**;6:2263-76
22. Xiong Z, Yu H, Ding Y, Feng C, Wei H, Tao S*, et al.* RNA sequencing reveals upregulation of RUNX1-RUNX1T1 gene signatures in clear cell renal cell carcinoma. Biomed Res Int **2014**;2014:450621
23. Zhou T, Luo M, Cai W, Zhou S, Feng D, Xu C*, et al.* Runt-Related Transcription Factor 1 (RUNX1) Promotes TGF-beta-Induced Renal Tubular Epithelial-to-Mesenchymal Transition (EMT) and Renal Fibrosis through the PI3K Subunit p110delta. EBioMedicine **2018**;31:217-25
24. Roseweir AK, Qayyum T, Lim Z, Hammond R, MacDonald AI, Fraser S*, et al.* Nuclear expression of Lyn, a Src family kinase member, is associated with poor prognosis in renal cancer patients. BMC Cancer **2016**;16:229
25. Lua J, Qayyum T, Edwards J, Roseweir AK. The Prognostic Role of the Non-Canonical Nuclear Factor-Kappa B Pathway in Renal Cell Carcinoma Patients. Urologia Internationalis **2018**;101:190-6
26. Kirkegaard T, Edwards J, Tovey S, McGlynn LM, Krishna SN, Mukherjee R*, et al.* Observer variation in immunohistochemical analysis of protein expression, time for a change? Histopathology **2006**;48:787-94
27. Qayyum T, McArdle PA, Lamb GW, Going JJ, Orange C, Seywright M*, et al.* Prospective study of the role of inflammation in renal cancer. Urol Int **2012**;88:277-81
28. Valente MJ, Henrique R, Costa VL, Jerónimo C, Carvalho F, Bastos ML*, et al.* A Rapid and Simple Procedure for the Establishment of Human Normal and Cancer Renal Primary Cell Cultures from Surgical Specimens. PLOS ONE **2011**;6:e19337
29. Fisher S, Barry A, Abreu J, Minie B, Nolan J, Delorey TM*, et al.* A scalable, fully automated process for construction of sequence-ready human exome targeted capture libraries. Genome biology **2011**;12:R1
30. Church DM, Schneider VA, Graves T, Auger K, Cunningham F, Bouk N*, et al.* Modernizing reference genome assemblies. PLoS Biol **2011**;9:e1001091
31. Cole AM, Ridgway RA, Derkits SE, Parry L, Barker N, Clevers H*, et al.* p21 loss blocks senescence following Apc loss and provokes tumourigenesis in the renal but not the intestinal epithelium. EMBO Mol Med **2010**;2:472-86
32. Growney JD, Shigematsu H, Li Z, Lee BH, Adelsperger J, Rowan R*, et al.* Loss of Runx1 perturbs adult hematopoiesis and is associated with a myeloproliferative phenotype. Blood **2005**;106:494-504
33. Ferrari N, Riggio AI, Mason S, McDonald L, King A, Higgins T*, et al.* Runx2 contributes to the regenerative potential of the mammary epithelium. Sci Rep **2015**;5:15658
34. Brugarolas J. Molecular genetics of clear-cell renal cell carcinoma. J Clin Oncol **2014**;32:1968-76
35. Fu Y, Sun S, Man X, Kong C. Increased expression of RUNX1 in clear cell renal cell carcinoma predicts poor prognosis. PeerJ **2019**;7:e7854
36. Nagy A, Lanczky A, Menyhart O, Gyorffy B. Validation of miRNA prognostic power in hepatocellular carcinoma using expression data of independent datasets. Sci Rep **2018**;8:9227
37. Hong D, Messier TL, Tye CE, Dobson JR, Fritz AJ, Sikora KR*, et al.* Runx1 stabilizes the mammary epithelial cell phenotype and prevents epithelial to mesenchymal transition. Oncotarget **2017**;8:17610-27
38. Keita M, Bachvarova M, Morin C, Plante M, Gregoire J, Renaud MC*, et al.* The RUNX1 transcription factor is expressed in serous epithelial ovarian carcinoma and contributes to cell proliferation, migration and invasion. Cell Cycle **2013**;12:972-86

694 39. Qin S, Shi X, Wang C, Jin P, Ma F. Transcription Factor and miRNA Interplays Can Manifest
695 the Survival of ccRCC Patients. Cancers **2019**;11
696 40. Peng ZG, Zhou MY, Huang Y, Qiu JH, Wang LS, Liao SH*, et al.* Physical and functional
697 interaction of Runt-related protein 1 with hypoxia-inducible factor-1alpha. Oncogene
698 **2008**;27:839-47
699 41. Kwon TG, Zhao X, Yang Q, Li Y, Ge C, Zhao G*, et al.* Physical and functional interactions
700 between Runx2 and HIF-1alpha induce vascular endothelial growth factor gene expression. J
701 Cell Biochem **2011**;112:3582-93
702 42. Lee SH, Che X, Jeong JH, Choi JY, Lee YJ, Lee YH*, et al.* Runx2 protein stabilizes hypoxia-
703 inducible factor-1alpha through competition with von Hippel-Lindau protein (pVHL) and
704 stimulates angiogenesis in growth plate hypertrophic chondrocytes. J Biol Chem
705 **2012**;287:14760-71
706 43. Tamiya H, Ikeda T, Jeong JH, Saito T, Yano F, Jung YK*, et al.* Analysis of the Runx2 promoter in
707 osseous and non-osseous cells and identification of HIF2A as a potent transcription
708 activator. Gene **2008**;416:53-60
709 44. Chen F, Zhang Y, Senbabaoglu Y, Ciriello G, Yang L, Reznik E*, et al.* Multilevel Genomics-Based
710 Taxonomy of Renal Cell Carcinoma. Cell Rep **2016**;14:2476-89
711 45. Geissler K, Fornara P, Lautenschlager C, Holzhausen HJ, Seliger B, Riemann D. Immune
712 signature of tumor infiltrating immune cells in renal cancer. Oncoimmunology
713 **2015**;4:e985082
714 46. Chang Y, An H, Xu L, Zhu Y, Yang Y, Lin Z*, et al.* Systemic inflammation score predicts
715 postoperative prognosis of patients with clear-cell renal cell carcinoma. British Journal Of
716 Cancer **2015**;113:626
717 47. de Vivar Chevez AR, Finke J, Bukowski R. The role of inflammation in kidney cancer. Adv Exp
718 Med Biol **2014**;816:197-234
719 48. Harlander S, Schonenberger D, Toussaint NC, Prummer M, Catalano A, Brandt L*, et al.*
720 Combined mutation in Vhl, Trp53 and Rb1 causes clear cell renal cell carcinoma in mice. Nat
721 Med **2017**;23:869-77
722 49. Nimmo R, Antebi A, Woollard A. mab-2 encodes RNT-1, a C. elegans Runx homologue
723 essential for controlling cell proliferation in a stem cell-like developmental lineage.
724 Development **2005**;132:5043-54
725 50. Robertson AJ, Coluccio A, Knowlton P, Dickey-Sims C, Coffman JA. Runx expression is
726 mitogenic and mutually linked to Wnt activity in blastula-stage sea urchin embryos. PLoS
727 One **2008**;3:e3770
728 51. Friedman AD. Cell cycle and developmental control of hematopoiesis by Runx1. J Cell Physiol
729 **2009**;219:520-4
730 52. Hoi CS, Lee SE, Lu SY, McDermitt DJ, Osorio KM, Piskun CM*, et al.* Runx1 directly promotes
731 proliferation of hair follicle stem cells and epithelial tumor formation in mouse skin. Mol Cell
732 Biol **2010**;30:2518-36
733 53. Blyth K, Slater N, Hanlon L, Bell M, Mackay N, Stewart M*, et al.* Runx1 promotes B-cell
734 survival and lymphoma development. Blood Cells Mol Dis **2009**;43:12-9
735 54. Cai X, Gao L, Teng L, Ge J, Oo ZM, Kumar AR*, et al.* Runx1 Deficiency Decreases Ribosome
736 Biogenesis and Confers Stress Resistance to Hematopoietic Stem and Progenitor Cells. Cell
737 Stem Cell **2015**;17:165-77
738 55. Kilbey A, Terry A, Wotton S, Borland G, Zhang Q, Mackay N*, et al.* Runx1 Orchestrates
739 Sphingolipid Metabolism and Glucocorticoid Resistance in Lymphomagenesis. J Cell Biochem
740 **2017**;118:1432-41
741 56. Xing Q, Huang Y, Wu Y, Ma L, Cai B. Integrated analysis of differentially expressed profiles
742 and construction of a competing endogenous long non-coding RNA network in renal cell
743 carcinoma. PeerJ **2018**;6:e5124

744 57. Qi Y, Zhang Y, Peng Z, Wang L, Wang K, Feng D*, et al.* SERPINH1 overexpression in clear cell
745 renal cell carcinoma: association with poor clinical outcome and its potential as a novel
746 prognostic marker. J Cell Mol Med **2018**;22:1224-35
747 58. Ito S, Nagata K. Biology of Hsp47 (Serpin H1), a collagen-specific molecular chaperone. Semin
748 Cell Dev Biol **2017**;62:142-51
749 59. Kim JI, Jang HS, Jeong JH, Noh MR, Choi JY, Park KM. Defect in Runx2 gene accelerates
750 ureteral obstruction-induced kidney fibrosis via increased TGF-beta signaling pathway.
751 Biochim Biophys Acta **2013**;1832:1520-7
752 60. Best S, Liu Y, Keikhosravi A, Drifka C, Woo K, Mehta G*, et al.* Collagen organization of renal
753 cell carcinoma differs between low and high grade tumors . 2019.
754 61. Du W, Zhang L, Brett-Morris A, Aguila B, Kerner J, Hoppel CL*, et al.* HIF drives lipid deposition
755 and cancer in ccRCC via repression of fatty acid metabolism. Nat Commun **2017**;8:1769
756 62. Rubin CI, Atweh GF. The role of stathmin in the regulation of the cell cycle. J Cell Biochem
757 **2004**;93:242-50
758 63. Illendula A, Gilmour J, Grembecka J, Tirumala VSS, Boulton A, Kuntimaddi A*, et al.* Small
759 Molecule Inhibitor of CBFbeta-RUNX Binding for RUNX Transcription Factor Driven Cancers.
760 EBioMedicine **2016**;8:117-31
761 64. Whittle MC, Izeradjene K, Rani PG, Feng L, Carlson MA, DelGiorno KE*, et al.* RUNX3 Controls
762 a Metastatic Switch in Pancreatic Ductal Adenocarcinoma. Cell **2015**;161:1345-60

763

764

765

766

767

768

769

770

771

772

773

774

775

776

777

778 ## Tables

Clinico-patholgical Characteristic	RUNX1 High n	%	RUNX1 Low n	%	P value
Age (≤61/>61)	21/24	(47/53)	68/70	(49/51)	0.211
Grade (I/II/III/IV)	2/16/17/10	(4/36/38/22)	11/38/65/19	(8/29/49/14)	0.332
T-Stage (I/II/III/IV)	22/6/15/2	(49/14/33/4)	57/24/48/4	(43/18/36/3)	0.802
Necrosis (not necrotic/necrotic)	3/19	(14/86)	8/38	(17/83)	0.861
Recurrence (no/yes)	30/16	(65/35)	106/32	(77/23)	0.121
Klintrup Makinen (Low/High)	13/33	(28/72)	76/62	(55/45)	**0.002**

779 **Table 1.** The relationship between RUNX1 and clinico-pathological characteristics of kidney cancer in
780 the TMA study.
781 All statistics Pearson Chi Square. Clinico-pathological scoring as previously published (24,25).
782
783
784
785
786
787
788
789
790
791
792
793

Figure Legends

Figure 1. cc*RCC patients with high RUNX1 expression have poorer survival.* A human tissue microarray containing 184 cores from ccRCC patients was stained for RUNX1. **a,** Representative examples of RUNX1 staining in non-tumour normal kidney and RCC cores. A range of RUNX1 expression was observed in ccRCC patients from negative to high. Magnified areas in dashed boxes, scale bar=100 pixels. **b,** Quantification of RUNX1 expression as shown by RUNX1 histoscore (H-Score) for the full TMA, the dashed red line represents the cut off for RUNX1 low (Quartile 1-3, H-Score: 0 to 26.7, n=138) and RUNX1 High (upper quartile, H-Score: 30 to 225, n=46). **c,** Kaplan-Meier curve showing reduced cancer specific survival in RUNX1 High patients, Log-rank P=0.007 (survival data was available for 183 patients, RUNX1 High n=45). The cumulative % survival for 5 years after diagnosis is shown below, Wilcoxon P=0.005. **d,** Average RUNX1 H-Score for patients divided into high Klintrup-Makinen score (KM High, average RUNX1 H-score=34.1) vs low Klintrup-Makinen score (KM Low, average RUNX1 H-score=15.2), t-test P=0.0027. **e,** % Distribution of KM Low and KM High patients in RUNX1 Low and High groups, RUNX1 Low: KM lo/hi %=55/45, RUNX1 High: KM lo/hi %=28/72, Chi-Square P=0.001.

Figure 2. *Deletion of RUNX1 causes a growth defect in human ccRCC cell lines.* **a,** Representative immunoblot for RUNX1 (inset) shows partial knockdown in 786-O cells stably transduced with two different shRUNX1 lentiviruses (786-O sh1 and 786-O sh5) compared to scrambled control (786-O Scr), re-probed for GAPDH loading control. shRUNX1 cells grow slower compared to Scr control in xCELLigence assay, N=4 independent experiments performed in quadruplicate. **b,** Cell index of 786-O shRUNX1 cells at 125h, *ANOVA P=0.0339; Scr vs sh5. **c,** Caki-2 ccRCC cells stably transfected with shRUNX1 (Caki-2 sh1 and Caki-2 sh5); average number of cells 96 hours after plating is shown; N=3 independent experiments, performed in triplicate, ANOVA P values: *sh1= 0.0226, **sh5= 0.0052. **d,** Representative Immunoblot for RUNX1 (inset) on 786-O vector control (pX Ctrl) and RUNX1 CRISPR cells (CRISPR A1 and CRISPR A3), re-probed for GAPDH loading control. 786-O RUNX1 CRISPR deleted

cells have a growth defect in xCELLigence assay, N=3 independent experiments, performed in quadruplicate. **e,** Cell index of RUNX1 CRISPR cells at 125h, ANOVA P values: **A1=0.0058, **A3=0.0025. **f,** Normalised cell counts of 786-O RUNX1 CRISPR cells compared to control at 96h after plating, N=4 independent experiments, performed in triplicate, ANOVA P values: **A1 P=0.0021 and **A3 P=0.0069. **g,** Representative flow cytometry plots for pX control and RUNX1 CRISPR clones (A1 and A3) time-point T6 (6 hours after 30 minute EdU pulse). Y axis is Log EdU-647 fluorescence, X axis is PI staining. Quadrants applied whereby Q1 and Q2 are EdU+ve and Q3 and Q4 are EdU-ve. Box represents G1* population. Numbers in quadrants are % of total single cells analysed. **h,** Average % of EdU+ve cells at T6. **i,** Average G1* % population of EdU+ve cells reveals G1* population is higher in pX control cells, ANOVA P values: ***A1 P= 0.0001 and *A3 P= 0.01. All flow cytometry are N=3 independent experiments performed in triplicate. **j,** Average number of SYTOX® green dead cells per well as a proportion of % confluence, ANOVA P values: A1= 0.0006, A3= 0.0015. N=4 independent experiments, performed in quadruplicate, analysed using Incucyte software. All error bars -/+ SEM.

Figure 3. *RUNX1 deleted cells have reduced in vitro cell migration and in vivo tumour formation.* **a,** Representative images of scratch wound closure (yellow) at 0, 12 and 24h after wounding for control and RUNX1 deleted 786-O cells. Scale bar=300mm. **b,** Quantification of wound closure as shown by relative wound density, ANOVA P values: A1 P= 0.0182, A3 P= 0.039. **c,** Relative wound density at 12h time-point is significantly reduced in RUNX1 deleted cells (A1 & A3), ANOVA P values: A1 P= 0.0164, A3 P= 0.0212. All scratch wound assays were performed in quadruplicate in 3 independent experiments, error bars are -/+ SEM. **d,** Representative ultrasound images of orthotopic recipient kidneys with 786-O* control and RUNX1-deleted cells over 18 weeks from surgery at indicated time-points. In control injected kidney the purple dashed line represents normal kidney outline, blue dashed line represents tumour outline. The proportion of tumour bearing kidneys as identified by ultrasound is presented below the panels for each time-point; p=0.011 (Fishers Exact test) at 18

weeks. **e,** H&E and IHC images of kidney tumours from control (n=4) and RUNX1-deleted (n=1) injected kidneys stained for RUNX1 and RUNX2, tumour areas indicated by arrows in H&E. The RUNX1-deleted injected kidney is negative for RUNX1 staining in the epithelium of the small tumour region whilst RUNX1 is still present in stromal cells, scale=100μm.

Figure 4. *RNA-sequencing reveals a RUNX1 dependant gene set in RCC cells.* **a,** Heatmap of genes in 786-O ccRCC cells that were identified from analysis of RNA-seq data as having significant differential expression (P<0.05; >2 fold change-FC), in the same direction between CRISPR clone A1 (n=3) and Control pX (n=3), and between CRISPR clone A3 (n=3) and Control pX. Blue represents down-regulation of gene expression (Row Z-Score <0) and red represents up-regulation of gene expression (Row Z-Score>0). Venn diagram of significantly differentially expressed (FC>2 and adjP<0.05) genes in CRISPR clone A1 (yellow) and clone A3 (purple) vs. Control and the overlap. 724 genes were significantly differentially expressed in both clones with 710 changed in the same direction in both, shown in brackets. Table of statistically significant pathways modulated in RUNX1 deleted 786-O cells compared to control, produced by Metacore (Clarivate Analytics) GeneGO analysis of RNA-seq data. P value and FDR (false discovery rate) shown. **b,** RNA-seq read counts of selected targets from the top pathway 'cell adhesion and ECM remodelling'. **c,** Volcano plot of average log2 fold change (x axis), versus –Log10 max adjusted P values (y axis). The average and max relate to values for both CRISPR clones A1 and A3. The points highlighted in red are the 724 differentially altered genes with average log2(Fold Change) >1 and Max(adjusted P values) <0.05. *STMN3* highlighted in red circle, *SERPINH1* highlighted in blue circle. **d,** Left: average read counts from RNA-seq data for STMN3 (upregulated +46.3x, P<0.0001) and SEPRINH1 (downregulated -4.1x, P<0.0001). Right: corresponding validation at the protein level, representative immuno-blot probed for STATHMIN3 and sequentially re-probed for SERPINH1 and GAPDH (loading control). **e,** RNA-seq read counts of

selected targets from the 2nd top pathway 'Eph and Ephrin signalling'. **f,** RNA-seq read count for *CPT1A*. Mean and SD of 3 biological replicates shown for all RNA-seq read counts, P values <0.0003.

Figure 5. *RUNX1 deletion delays kidney cancer in a genetic mouse model.* **a,** Representative images of two normal kidneys and kidney tumours from the *AH-Cre;Apc$^{fl/fl}$;p21$^{-/-}$* (referred to as *CAP*) genetic mouse model of kidney cancer stained for RUNX1 (scale bar=100µm). **b,** Immunohistochemistry (IHC) for RUNX1 in two representative kidney tumours from *CAP;Runx1$^{fl/fl}$* mice confirms deletion of RUNX1 in the tumours. **c,** Kaplan-Meier survival curve for *CAP;Runx1$^{+/+}$* vs *CAP;Runx1$^{fl/fl}$* mice showing improved survival on *Runx1* deletion, Log-rank P=0.0365. **d,** Mean average lifespan for *CAP;Runx1$^{+/+}$* (78.6 days, n=16) vs *CAP;Runx1$^{fl/fl}$* mice (104.6 days, n=19), t-test P=0.0415. **e,** Representative images of two different *CAP;Runx1$^{+/+}$* and *CAP;Runx1$^{fl/fl}$* tumours (n1 and n2) stained for the proliferation marker Ki67 (scale bar=100µm). **f,** Quantification by HALO analysis of the % of Ki67+ cells, *Runx1$^{+/+}$*=34% (n=12), *Runx1$^{fl/fl}$*=24.4% (n=9), t-test P=0.0154. **g,** Representative IHC images of tumours (4 vs 4) from *CAP;Runx1$^{+/+}$* vs *CAP;Runx1$^{fl/fl}$* mice stained for SERPINH1.

Figure 6. *RUNX2 is expressed in human RCC and correlates with poorer survival.* **a,** Serial sections from *CAP;Runx1$^{+/+}$* and *CAP;Runx1$^{fl/fl}$* murine kidney tumours immuno-stained for both RUNX1 and RUNX2 show high RUNX2 expression in both cohorts. Magnified section in dashed boxes, scale bars=100µm. *CAP* mice are *AH-Cre;Apc$^{fl/fl}$;p21$^{-/-}$*. **b,** Representative examples of RUNX2 staining in non-tumour normal kidney and RCC cores from human TMA as used in Fig1. A range of RUNX2 expression was observed in RCC patients from negative to high. Magnified areas in dashed boxes, scale bars=100µm. **c,** Kaplan-Meier curve showing reduced cancer specific survival in RUNX2 High patients, Log-rank P=0.0478 and inset life table showing cumulative % survival for 5 years after diagnosis, Wilcoxon P=0.045. **d,** RUNX2 H-Score is significantly higher in patients with a high KM

894 score (KM Low=5.3, KM High=16.1, t-test p=0.0005). **e,** Proportion of KM Low and KM High patients

895 in RUNX2 Low and High groups, RUNX2 Low KM lo/hi %=57/43, RUNX2 High KM lo/hi %=28/72.

896

897

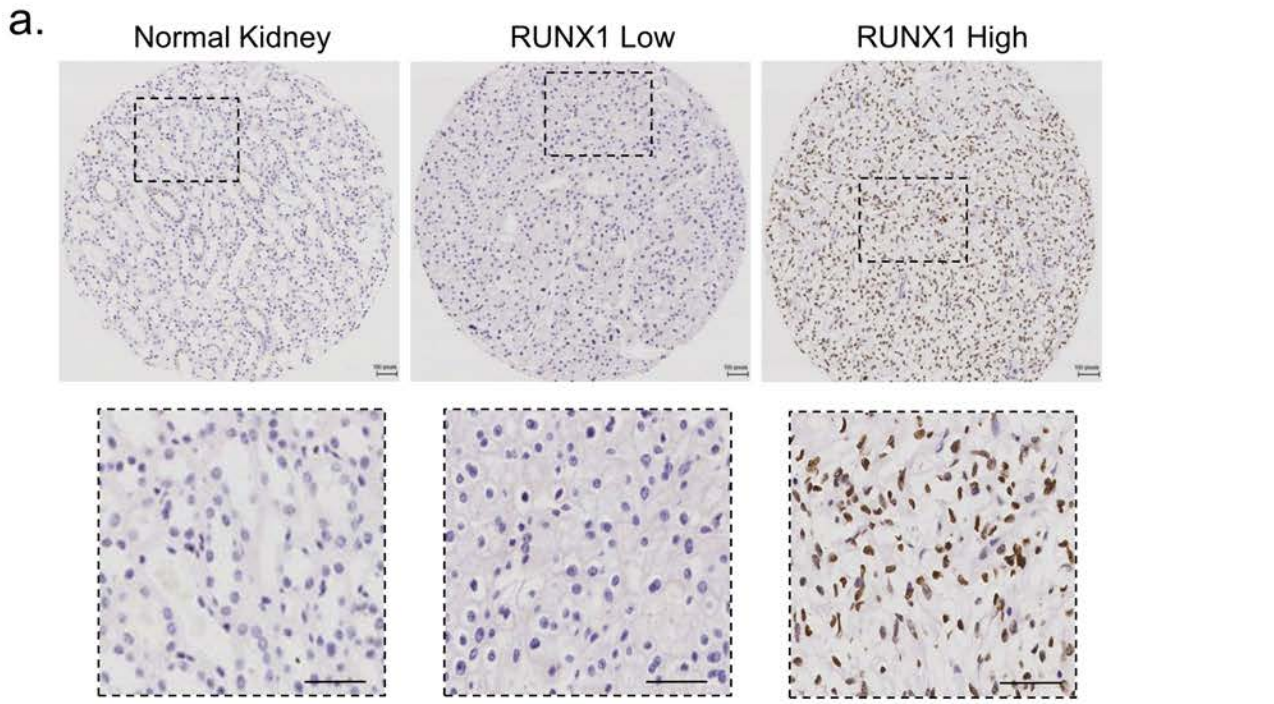

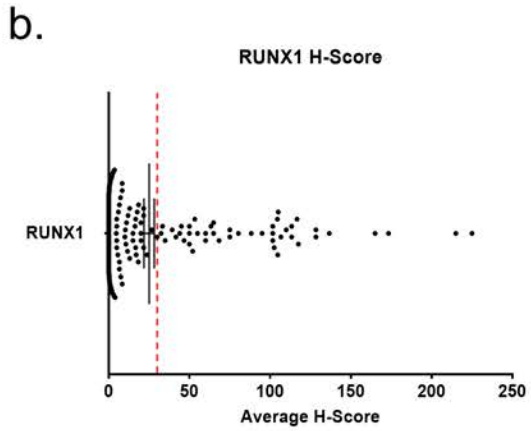

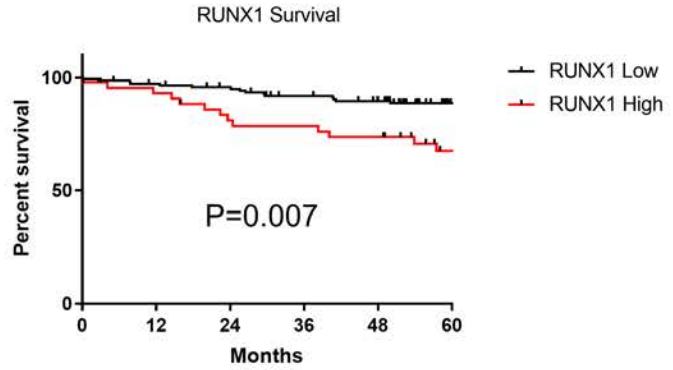

RUNX1 status	Cumulative survival (%)				
	1yr	2yr	3yr	4yr	5yr
RUNX1 Low (n=138)	97	96	92	89	88
RUNX1 High (n=45)	93	81	79	74	68

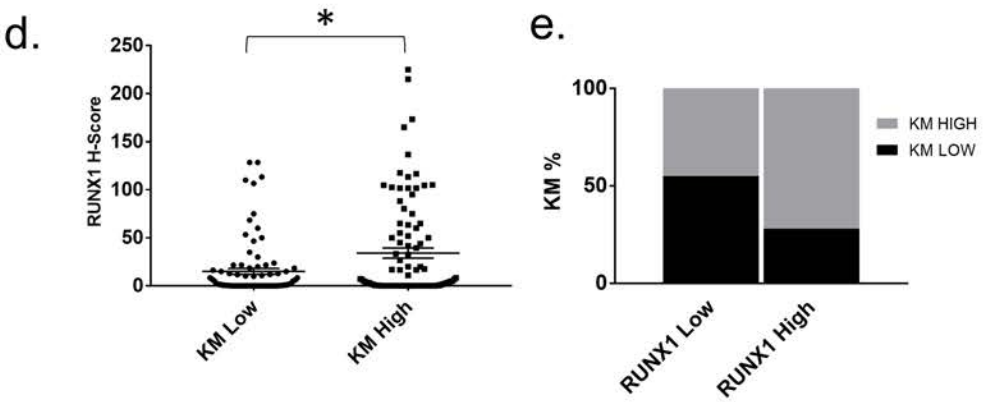

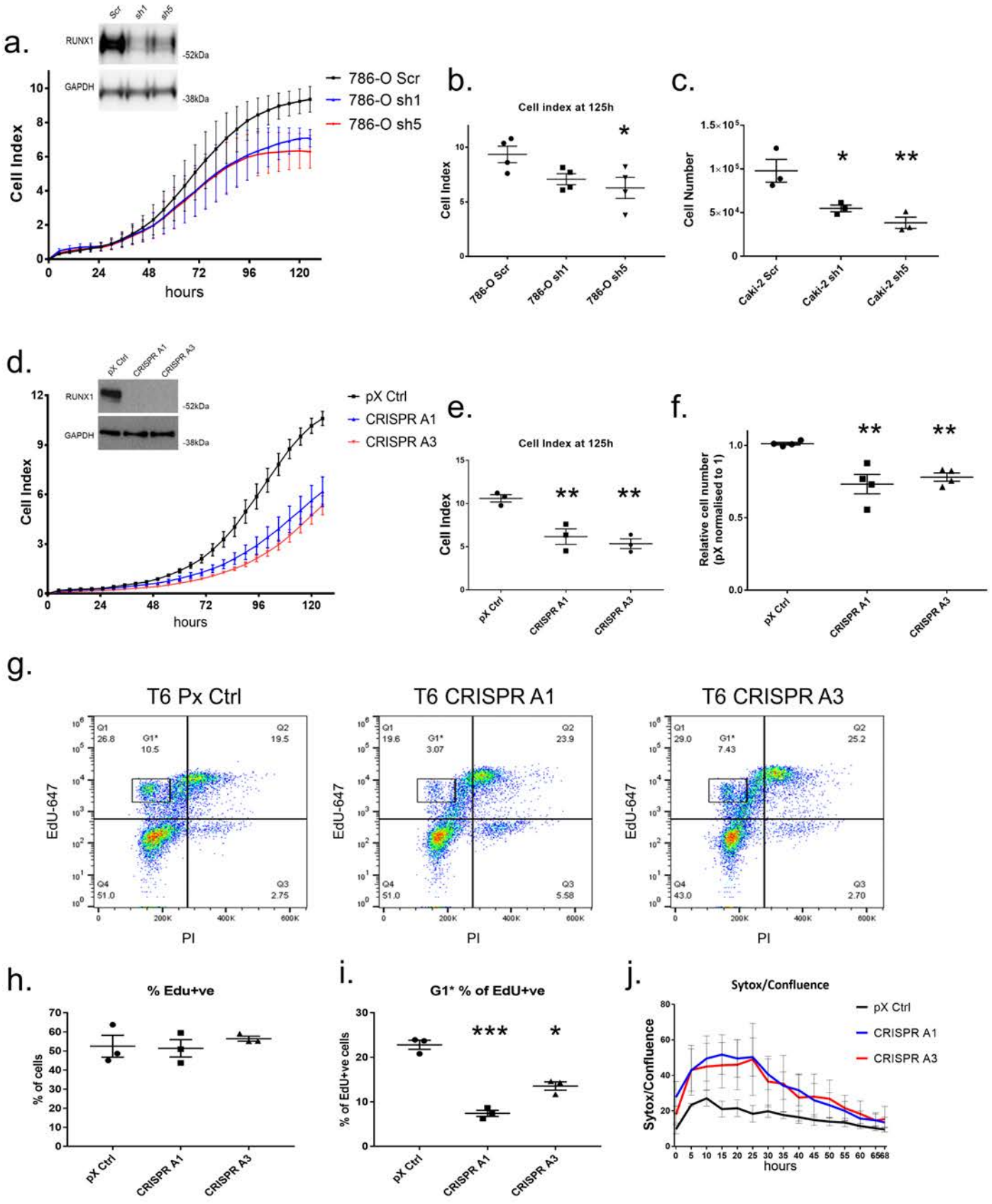

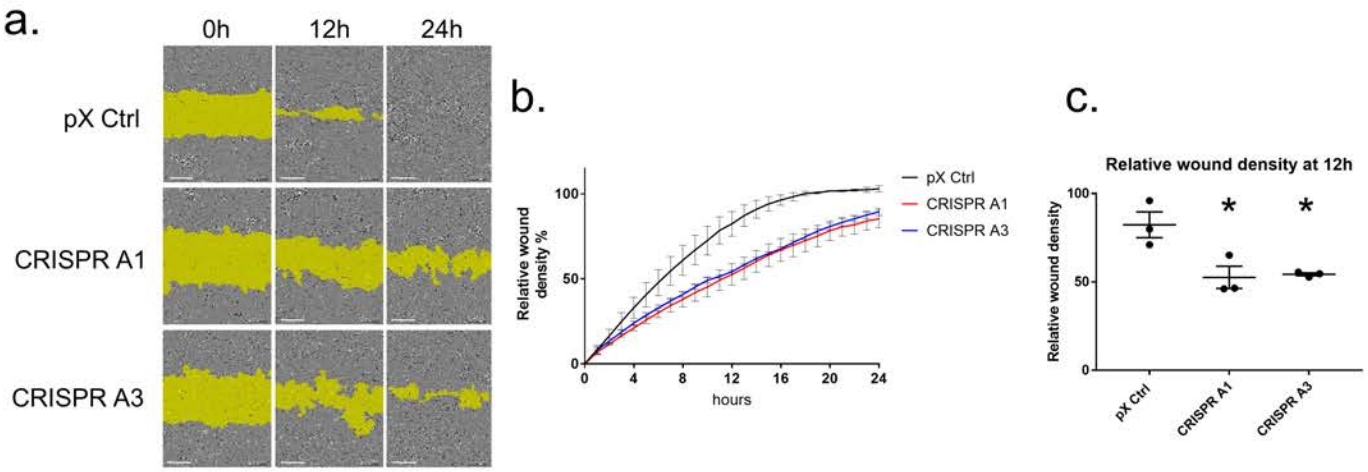

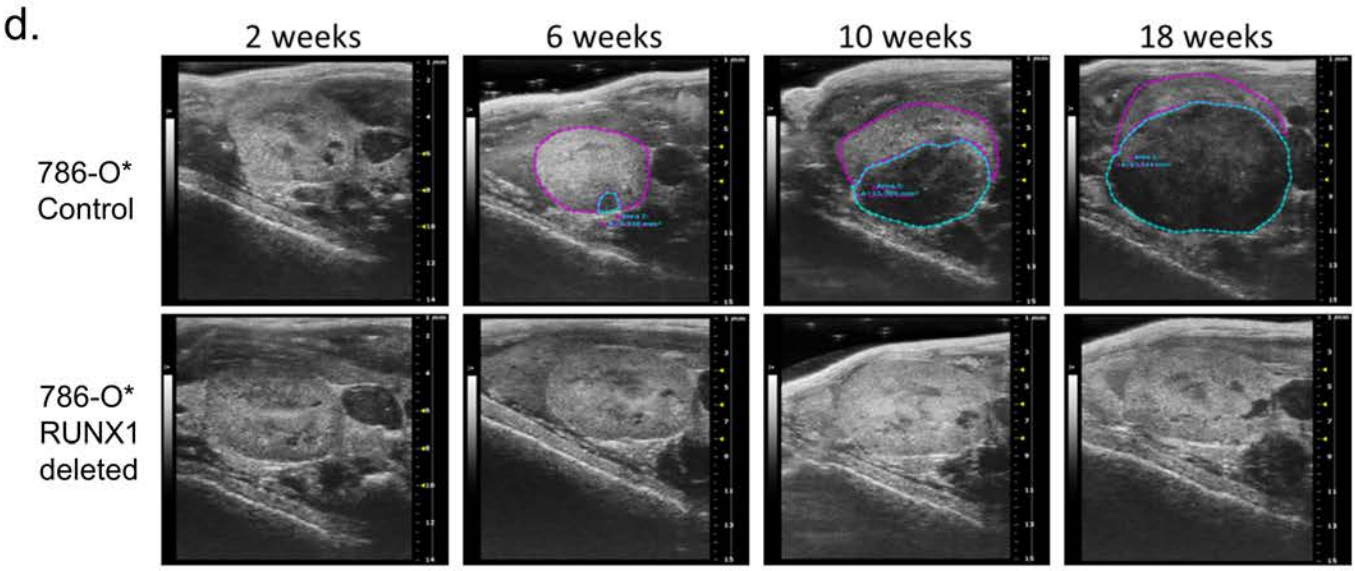

	2 weeks	6 weeks	10 weeks	18 weeks
786-O* Control	0/13	2/13	7/13	8/13
786-O*RUNX1 deleted	0/13	0/13	0/13	1/13

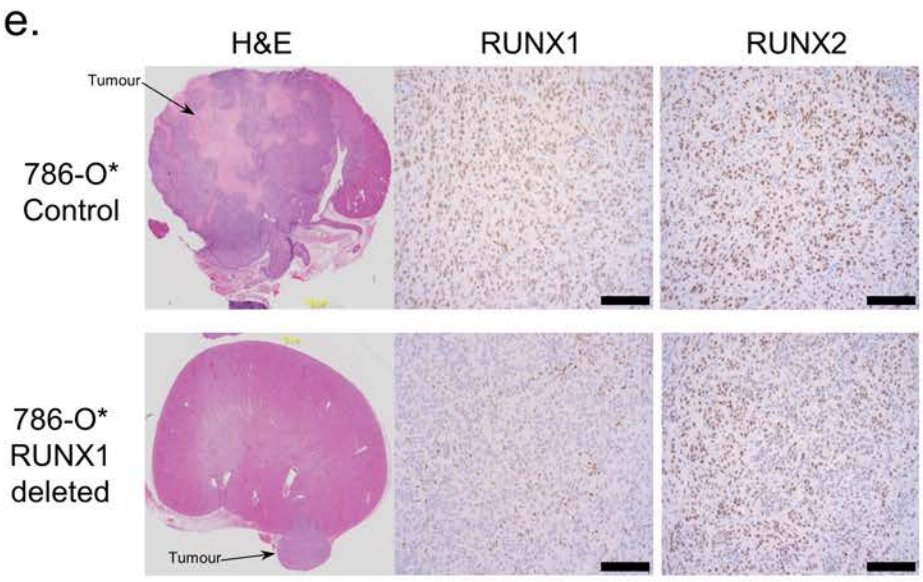

Rooney et al

Figure 3

a.

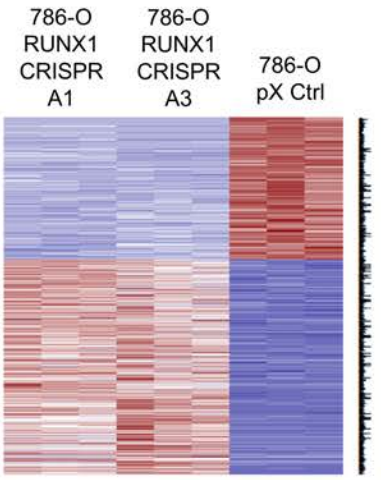

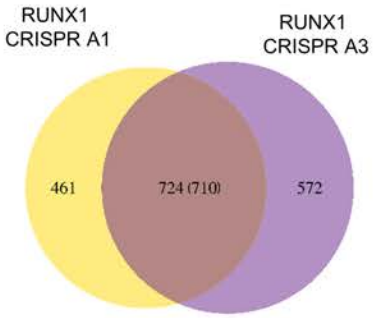

Rank	Regulated Pathway	P-value	FDR
1	Cell adhesion ECM remodelling	6.001E-06	6.362E-03
2	Inhibition of Ephrin receptors in colorectal cancer	6.932E-05	3.265E-02
3	Role of cell adhesion molecules in progression of pancreatic cancer	9.310E-05	3.265E-02
4	Langerhans cell migration to lymph nodes in allergic contact dermatitis	1.712E-04	3.265E-02
5	Transport The role of AVP in regulation of Aquaporin 2 and renal water	1.848E-04	3.265E-02
6	Angiogenesis in HCC	1.848E-04	3.265E-02
7	Role of red blood cell adhesion to endothelium in vaso-occlusion in sickle cell disease	2.354E-04	3.565E-02
8	Glutathione metabolism	3.023E-04	4.005E-02
9	CHDI Correlations from Replication data causal network (negative correlations)	3.658E-04	4.308E-02

b.

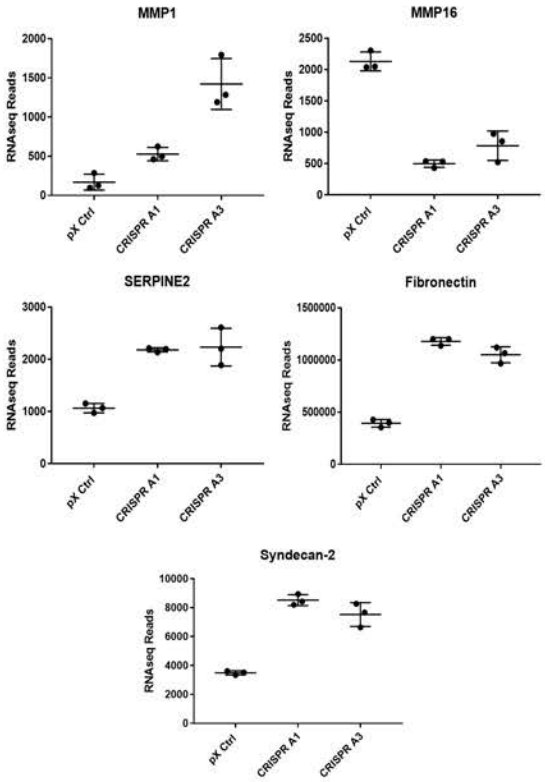

c.

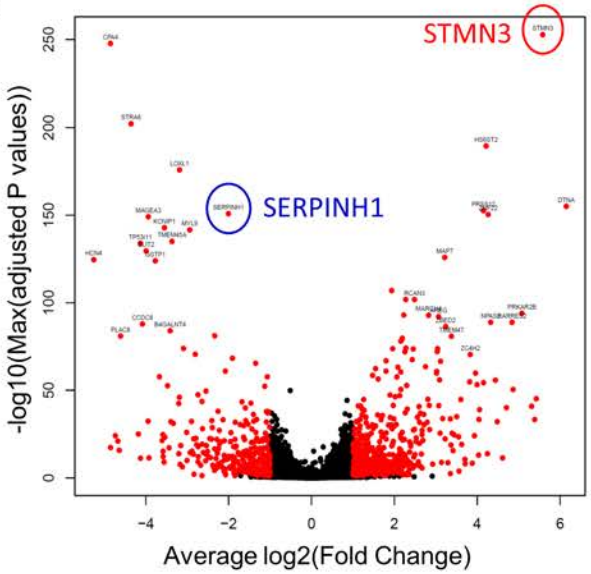

d.

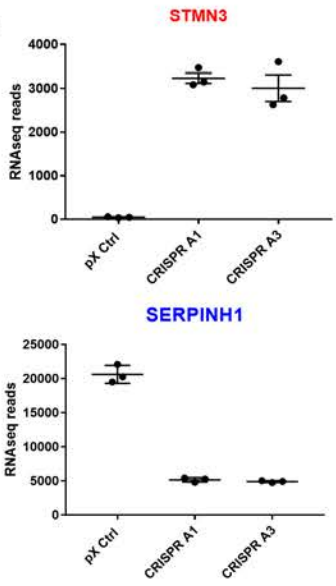

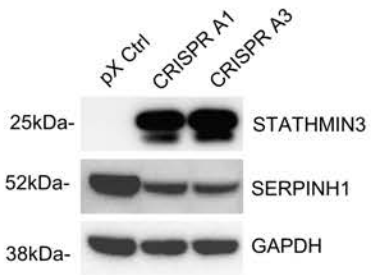

e.

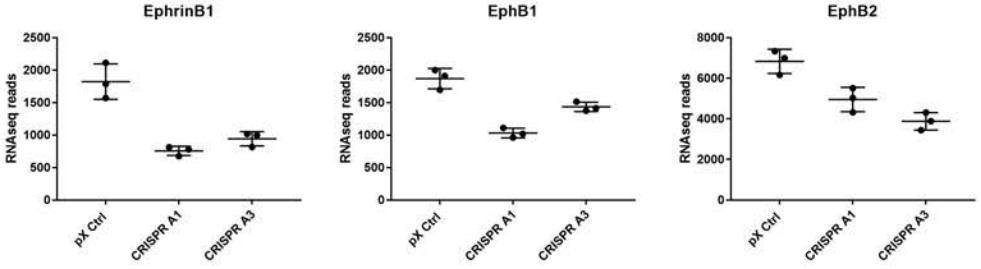

f.

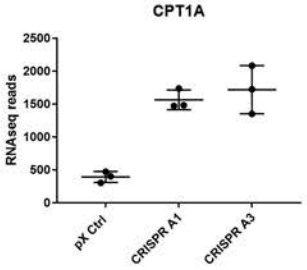

Author Manuscript Published OnlineFirst on March 10, 2020; DOI: 10.1158/0008-5472.CAN-19-3870
Author manuscripts have been peer reviewed and accepted for publication but have not yet been edited.

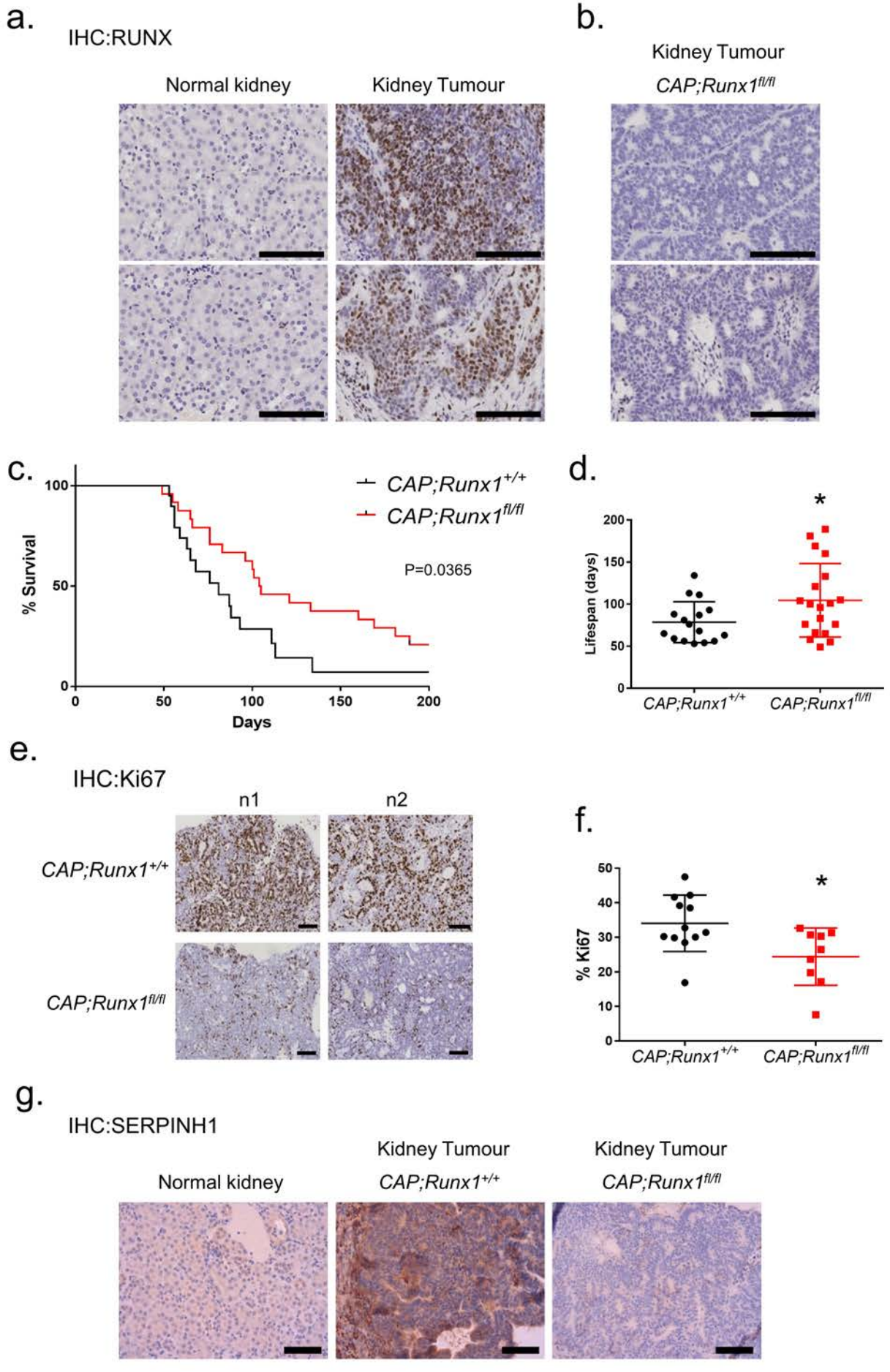

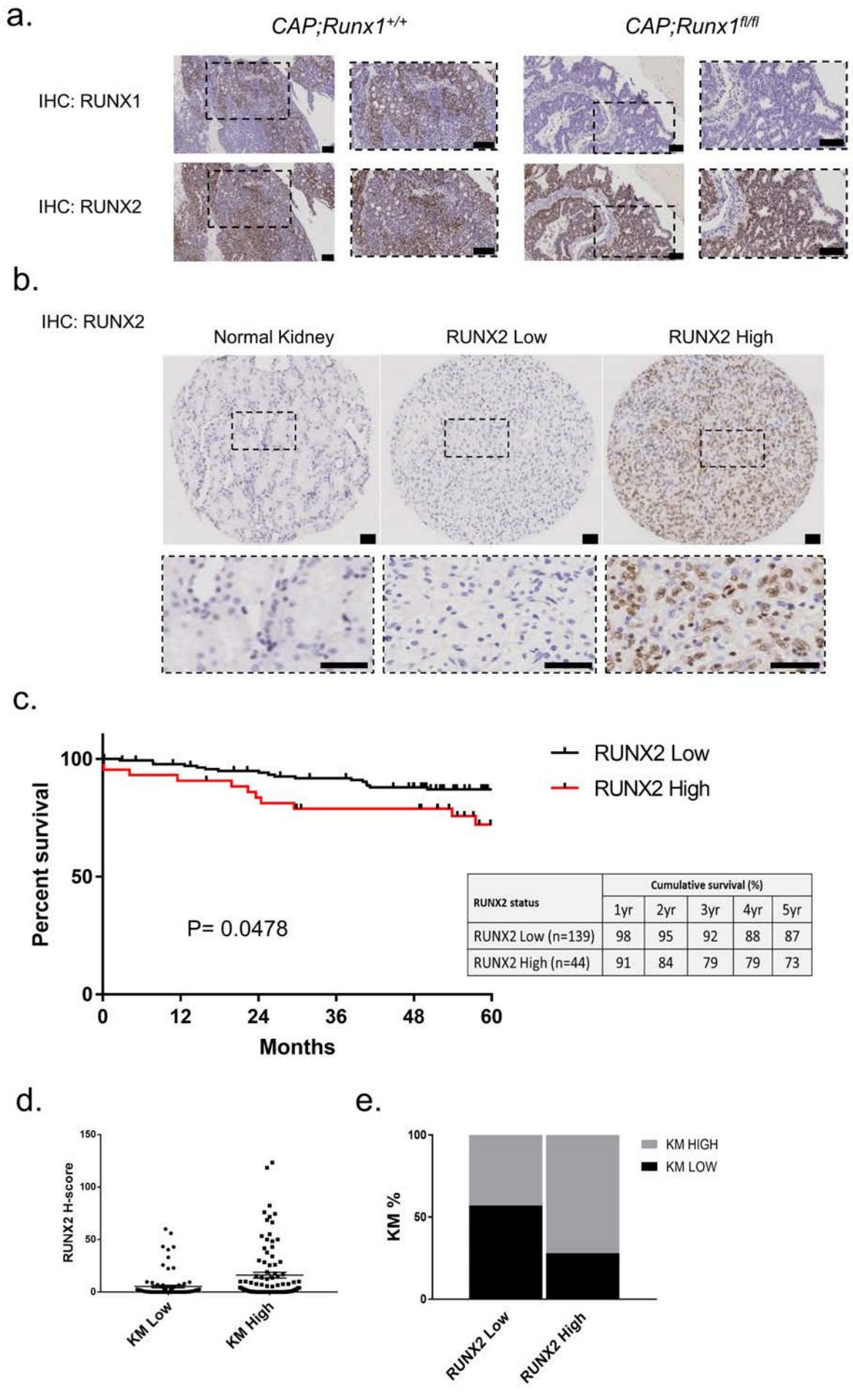

Figure 6

AACR American Association for Cancer Research

Cancer Research

The Journal of Cancer Research (1916–1930) | The American Journal of Cancer (1931–1940)

RUNX1 is a driver of renal cell carcinoma correlating with clinical outcome

Nicholas Rooney, Susan M Mason, Laura McDonald, et al.

Cancer Res Published OnlineFirst March 10, 2020.